Crystallisation history of thyolites at long Valley, California, inferred from combined U-series and Rb-Sr isotope systematics

Heumann, A.; Davies, G.R.; Elliott, T.R.

published in
Geochimica et Cosmochimica Acta
2002

DOI (link to publisher)
10.1016/S0016-7037(01)00883-3

document version
Publisher's PDF, also known as Version of record

Pergamon

Geochimica et Cosmochimica Acta, Vol. 66, No. 10, pp. 1821–1837, 2002

0016-7037/02 $22.00 + .00

PII S0016-7037(01)00883-3

Crystallization history of rhyolites at Long Valley, California, inferred from combined U-series and Rb-Sr isotope systematics

ARND HEUMANN,[1,*] GARETH R. DAVIES,[1] and TIM ELLIOTT[1,2]

[1]Faculteit der Aardwetenschappen, Vrije Universiteit Amsterdam, De Boelelaan 1085, 1081 HV Amsterdam, The Netherlands
[2]Department of Earth Sciences, University of Bristol, Wills Memorial Building, Queen's Road, Bristol BS8 1RJ, United Kingdom

(*Received November* 14, 2000; *accepted in revised form November* 8, 2001)

Abstract—In this study, we present $^{87}Rb/^{86}Sr$ and $^{230}Th/^{238}U$ isotope analyses of glasses and phenocrysts from postcaldera rhyolites erupted between 150 to 100 ka from the Long Valley magmatic system. Both isotope systems indicate complex magma evolution with preeruptive mineral crystallization and magma fractionation, followed by extended storage in a silicic magma reservoir. Glass analyses yield a Rb-Sr isochron of 257 ± 39 ka, which can be explained by a feldspar-fractionation event ~150 ky before eruption. Individual feldspar–glass pairs confirm this age result. A mineral ^{230}Th-^{238}U isochron in a low-silica rhyolite from the Deer Mountain Dome defines an age of 236 ± 1 ka, but the glass and whole rock do not lie on the isochron. U-Th fractionation of the rocks is controlled by the accessory minerals zircon and probably allanite, which crystallized at 250 ± 3 ka and 187 ± 9 ka, respectively. All major mineral phases contain accessory mineral phases; therefore, the mineral isochron represents a mixture of zircon and allanite populations. A precision of ±1 ka for the mixing array implies that the minor phases must have crystallized within this timescale. Longer periods of crystal growth would cause the mixing array to be less well defined. U-series data from other low- and high-silica rhyolites indicate younger accessory mineral crystallization events at ~200 and 140 ka, probably related to the thermal evolution of the magma reservoir. These crystallization events are, however, only documented by the accessory minerals and had no further influence on bulk magma compositions. We interpret the indistinguishable age results from both isotope systems (~250 ka) to record the fractionation of small magma batches by filter pressing from a much larger underlying magma volume, followed by physical isolation and extended storage at the top of the magma reservoir for up to 150 ky. *Copyright © 2002 Elsevier Science Ltd*

1. INTRODUCTION

The volcanic hazard of voluminous, long-lived silicic systems such as Yellowstone and Long Valley is well recognized (Spera and Crisp, 1981; Shaw, 1985). Such high-silica volcanic systems (>75 wt% SiO_2) produce some of the largest and most destructive eruptions on Earth (Simkin, 1993) and are characterized by long periods of quiescence between large eruptions, a behavior interpreted as the gradual buildup of magma volumes between periods of major activity. A key issue, therefore, is to place absolute constraints on the rates of magma chamber processes that form highly fractionated rhyolitic magmas and to predict the evolution of explosive, batholith-sized silicic magma systems.

The $^{230}Th/^{238}U$, and in some circumstances Rb-Sr, isotope systems represent chronometers that can constrain the timescales over which different physical processes operate during rhyolite genesis (e.g., Halliday et al. 1989; Reid et al., 1997). Combined application of these chronometers to rhyolites that are young enough for the U-Th disequilibrium method (<350 ky) and have low Sr contents and consequently high Rb/Sr ratios is a potentially powerful approach because the two isotope systems respond in markedly different ways to magmatic processes. Comparison of the isotope systems therefore provides complementary perspectives on the timescales of magma evolution. To separate preeruptive from posteruptive aging, a further high-precision chronometer is required to accurately date the eruptions. For this purpose, laser-fusion ^{40}Ar-^{39}Ar dating of sanidines is used.

In this study, we place absolute age constraints on the rates of magma chamber processes that formed the ~110-ka postcaldera rhyolites of the Long Valley, California, magmatic system. Our aim is to determine the time of mineral crystallization, the rates at which magmas are fractionated and modified, and the duration of storage in magma chambers.

2. GEOLOGICAL BACKGROUND

The Long Valley magmatic system is situated at the northern end of Owens Valley, California, at the eastern front of the Sierra Nevada. A large silicic magma chamber has produced evolved rhyolites over the last 2.1 Myr (Bailey et al., 1976). During the initial 1.3-Myr period, >50 km^3 of high-silica rhyolites (HSR) were erupted at Glass Mountain, northeast of the current caldera structure (Metz and Mahood, 1985). The first magmatic stage culminated in the formation of the Long Valley caldera at 760 ka with the catastrophic eruption of the voluminous (>600 km^3), chemically zoned Bishop Tuff (Hildreth, 1979; Pringle et al., 1992). Following eruption of the Bishop Tuff, magmatism continued to be of predominantly rhyolitic composition (Bailey et al., 1976; Mankinen et al., 1986; Bailey, 1989; Heumann and Davies, 1997). Early postcaldera rhyolites (>75 km^3) were erupted between 750 and 650 ka, forming a resurgent dome (Fig. 1). After a quiescent period of ~100 ky, three groups of more crystal-rich moat rhyolites

* Author to whom correspondence should be addressed (heua@geo.vu.nl).

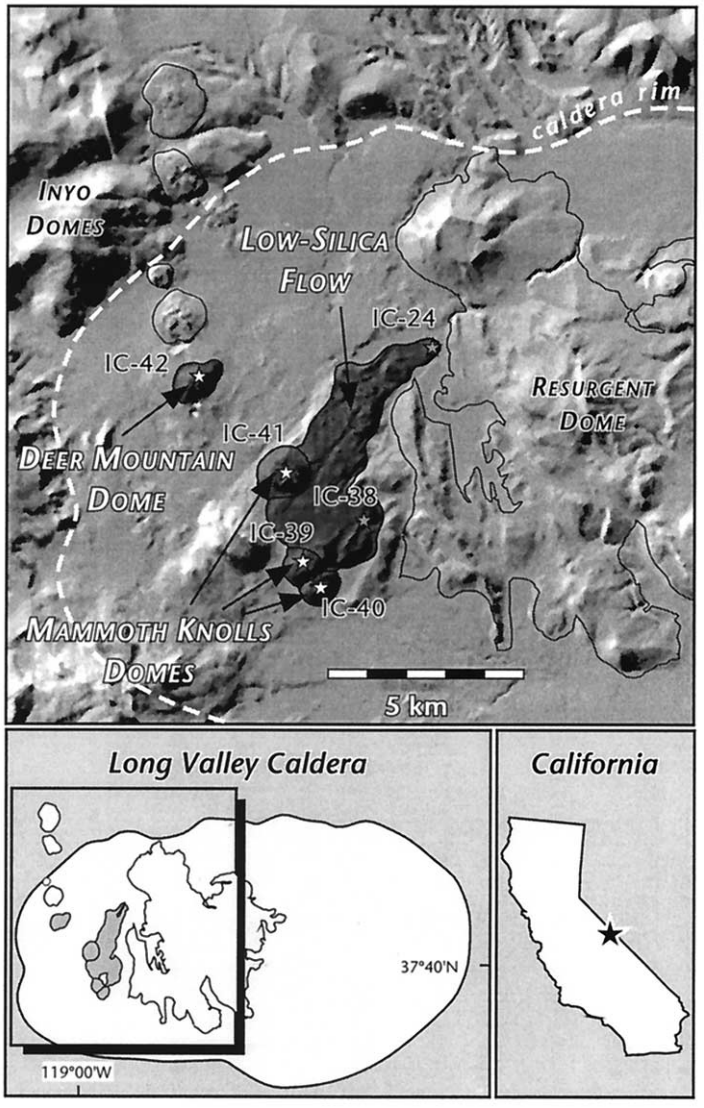

Fig. 1. Sample location map of rhyolitic postcaldera units from the southwest moat of the Long Valley caldera. The three rhyolitic domes of Mammoth Knolls and Deer Mountain erupted at ~110 ka at the fringes of a large low-silica flow (star symbols = sample locations). For further details of the postcaldera magmatism, see Bailey (1989) and Heumann and Davies (1997).

erupted at ~200-ky intervals. Initial magmatism was to the north of the resurgent dome, but activity migrated clockwise around the resurgent dome (Bailey, 1989). The youngest moat rhyolites (~110 ka) are the focus of this study. They are contemporaneous with part of a more protracted period of basaltic and quartz–latitic lavas (200 to 50 ka) in the west moat of the caldera (Mankinen et al., 1986; Bailey, 1989; Vogel et al., 1994; Cousens, 1996). The Inyo Craters form a north–south chain of recent domes, which are the youngest expression of rhyolitic volcanism in the Long Valley region.

The postcaldera rhyolites have compositions that define a large and continuous compositional range from low to high-silica rhyolite (72 to 77%). All the rhyolites lie on a well-defined Pb-Sr isotope mixing array between lavas of the ~700-ka resurgent dome and the Recent Inyo lava domes (Fig. 2). The systematic temporal variations in Pb and Sr isotope ratios establish that compared with the sampling interval of ~50 ky, there was near-continuous addition of a siliceous magma to a chamber that contained magma residual after eruption of the Bishop Tuff (Heumann and Davies, 1997). The decrease in $^{87}Sr/^{86}Sr$ ratios with time, even in rocks with low Sr contents, is evidence that once in the magma chamber, magmas do not undergo significant crustal interaction. Heumann and Davies (1997) postulated that at ~400 ka, the magma chamber became stratified with chemically more evolved HSR overlying a well-mixed body of low-silica rhyolite (LSR). They further argued, on the basis of the temporal evolution of the Sr isotope ratios, that HSR were stored in the upper section of the magma chamber for up to 200 ky before eruption. This work is designed to test this model and to see if the detailed crystallization history of these postcaldera rhyolites provides an explanation for the origin of the >100-ky preeruptive mineral ages reported by Reid et al. (1997) and Heumann and Davies (1997).

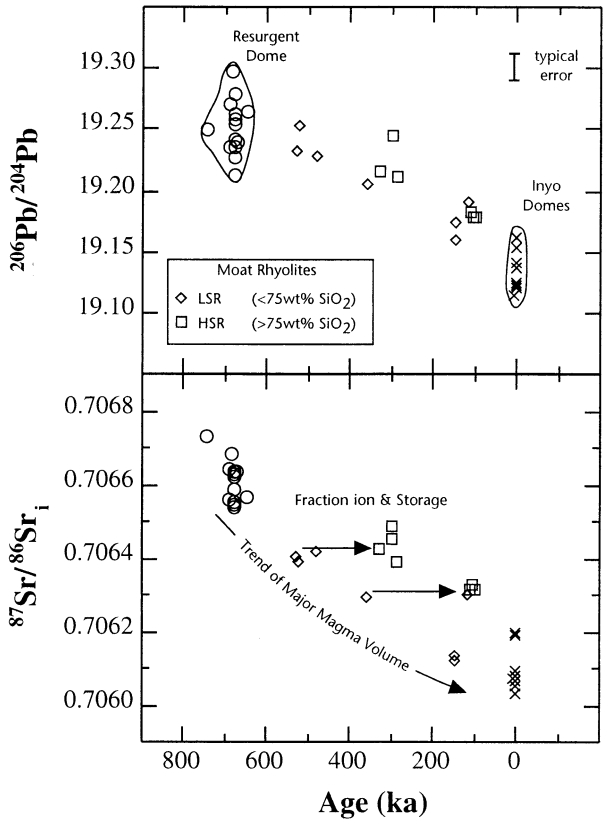

Fig. 2. Temporal variations of Sr-Pb isotopes in postcaldera rhyolites of the Long Valley magmatic system (Heumann and Davies, 1997). The isotopic data imply an open-system with semicontinuous addition of material to a residual magma chamber (resurgent dome) with less radiogenic Pb and Sr isotope ratios (i.e., Inyo Domes). Arrows indicate how certain small volumes of rhyolites can be compared with the major magma volume before fractionation and extended isolation at the top of the magma chamber.

3. SAMPLES

Rhyolitic domes and flows that erupted between 150 and 100 ka were selected for investigation of their crystallization history (Fig. 1). The samples comprise two LSR lava flows from locations north of Mammoth Lakes (IC-24, 38), the LSR Deer Mountain Dome (IC-42), and three HSR Mammoth Knolls Domes (IC-39, 40, 41). The samples are sparsely porphyritic, light-gray-colored rocks with a glassy (~80 to 95%) pumiceous matrix and variable mineral contents. Phenocrysts are quartz, sanidine, plagioclase, biotite, hornblende, and clinopyroxene. In the HSR, felsic minerals vary from 3 to 15%, and mafic minerals are generally <1%. The LSRs have higher phenocryst contents up to ~20%, with approximately 3% mafic minerals. Phenocrysts are generally euhedral; only plagioclase shows weak compositional zonations.

Accessory minerals comprise zircon, allanite, magnetite, apatite, ilmenite, and pyrrhotite, in decreasing order of abundance. The scanning electron microscope (SEM) images in Figure 3 summarize the spectrum of zircon morphologies in the mineral separates. Zircon occurs in several habits: 10- to 30-μm grains within or attached to major mineral phases; glomerophyric clots (50 μm); or solitary crystals (50 to 300 μm). The largest zircon grains are light gray and invariably have inclusions of much smaller zircon and apatite grains (Fig. 3d). Allanite occurs as large euhedral grains (100 to 500 μm) and smaller mineral inclusions (10 to 50 μm) in amphibole and biotite (Figs. 3e,f). Ilmenite, pyrrhotite, and apatite are present as inclusions in all accessory minerals. Magnetite typically forms small spherical inclusions in biotite. Pyrrhotite was only identified as inclusions in allanite. Observations of accessory phases were made on several thin sections and on grain mounts of heavy-density mineral fractions. Only the largest zircons, the main accessory phase, yielded sufficient material for U-series isotopic analysis.

4. ANALYTICAL PROCEDURES

Between 30 and 100 mg of mineral grains and glasses were hand-picked after density and magnetic separation. The major mineral phases probably contain inclusions of accessory phases because SEM analysis shows that they are ubiquitous, but no clear optical distinction could be made during hand picking. For U-Th analyses of zircon, approximately five pristine large grains (100 to 200 μm) were selected; only sample IC-39 consists of a composite separate of varying grain sizes (~50 to 200 μm). For Rb-Sr, U-Th, and Pb analysis, cleaned glasses, feldspars, biotite, and hornblende separates were dissolved in sealed Teflon beakers with a HF-HNO_3-$HClO_4$ mixture. Zircon separates underwent the same procedure except that dissolutions were performed in Teflon-lined acid digestion bombs at 220°C. Sample solutions were then split into spiked and unspiked aliquots for sequential Pb-Sr-Rb separation by standard chromatographic ion-exchange techniques. Mixed ^{87}Rb-^{84}Sr spikes were used for determination of Rb and Sr concentrations by isotope dilution. Both isotopic compositions and elemental concentrations for Th and U were determined on a single aliquot with a mixed ^{229}Th-^{233}U spike. Chromatographic separation of Th and U involved successive elutions on 0.5- and 0.17-mL anionic resin columns with a standard HNO_3-HCl-H_2O scheme. The total procedural blanks for Pb, Sr, U, and Th were <200, <250, <30, and <13 pg.

Rb isotope dilution measurements were made on a MAT 261 mass spectrometer. Multiple measurements of a natural Rb standard indicated a mass discrimination factor of 0.15 ± 0.05% (n = 10) per atomic mass unit, which was used to correct for mass fractionation. Pb, Sr, U, and Th isotope compositions were analyzed on a MAT 262 RPQ+ mass spectrometer. All Pb isotope measurements were performed in a single analytical session. Correction for mass fractionation of the static Pb measurements is based on a discrimination factor of 0.117 ± 0.008% (n = 5) per atomic mass unit obtained from multiple measurements of NBS 981. Sr isotope ratios were measured dynamically and corrected for mass fractionation following an exponential law based on ^{86}Sr/^{88}Sr = 0.1194. During the course of analyses, the mean value for NBS 987 was 0.710234 ± 16 (n = 12).

For Th isotope measurements, two consecutive series of data collection were performed on the same filament load with a ^{229}Th "bridge" to negate any effects of energy filter drift. To allow this, samples were spiked so as to yield a ^{232}Th/^{229}Th ~1000. The first data collection used the ion counter behind the RPQ energy filter to determine a ^{232}Th/^{229}Th ratio by peak

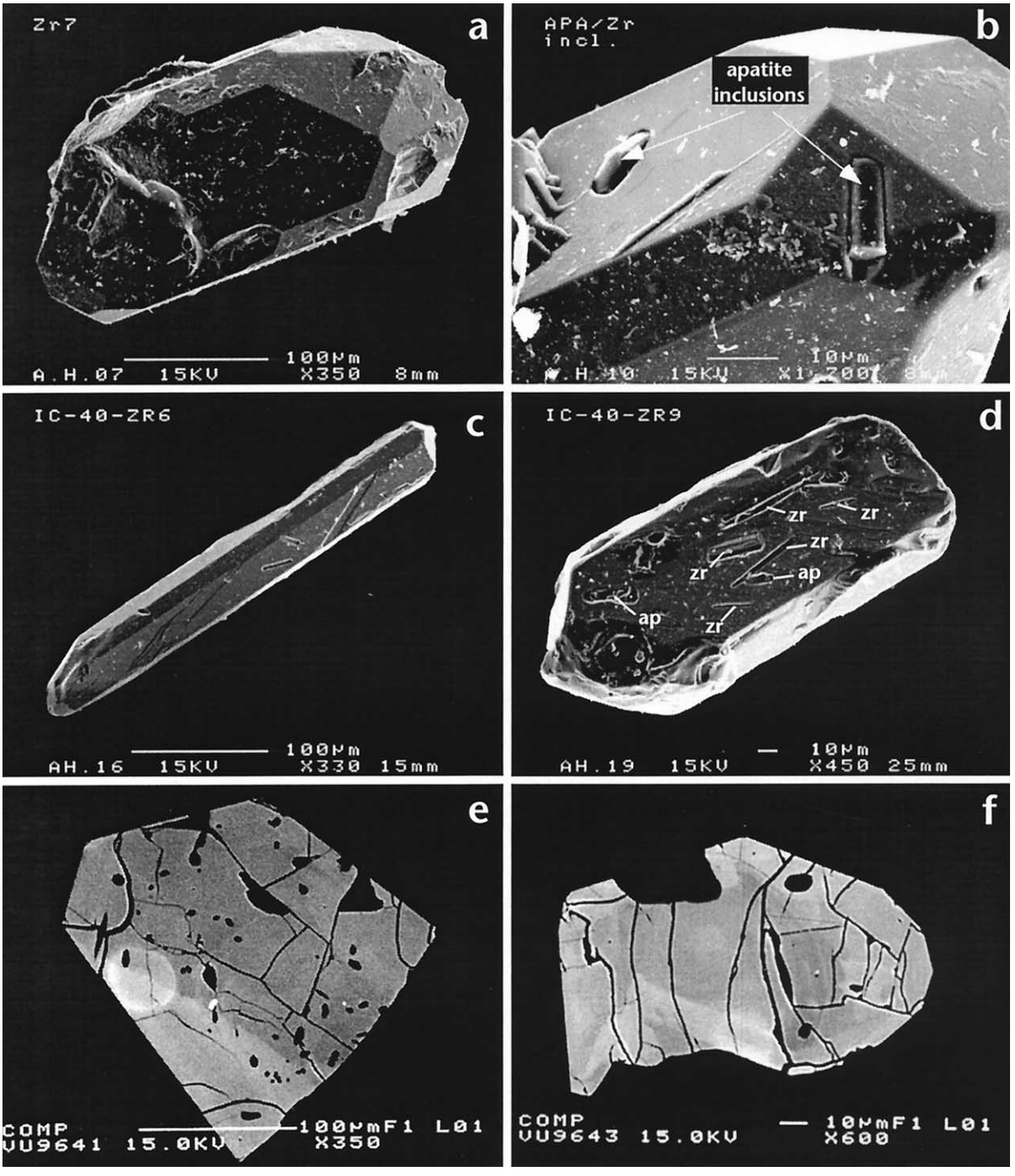

Fig. 3. SEM images of different zircon populations and backscattered-electron images of allanite crystals. (a,b) LSR IC-42 of Deer Mountain. A group of large zircons (~300 μm) comprise both prismatic elongated and stubby euhedral phenocrysts. A subset of zircons with identical morphologies can be found in the 10- to 100-μm range as either inclusions in the larger grains or discrete grains in the glass. The large zircon grains of the medium-sized morphology show inclusions of a third and smallest group of zircons (b). These zircons are commonly $<$30 μm in size and occur together with apatite. (c,d) HSR IC-40 of the Mammoth Knolls Domes. In general, the distribution of different sized zircon morphologies appears to be similar in LSR and HSR. Elongation ratios (length/width) seem to become larger in HSR samples with more needle-shaped and prismatic zircons (c). The crystal in (d) shows variable-sized zircon and apatite inclusions along a crystal face that probably represents the contact to another mineral phase, to which the zircon was previously attached or intergrown. (e,f) Zoned allanite crystals from the LSR flow (IC-24) and the HSR Mammoth Knolls Dome (IC-39). Inclusions in allanite are glass, zircon, and pyrrhotite.

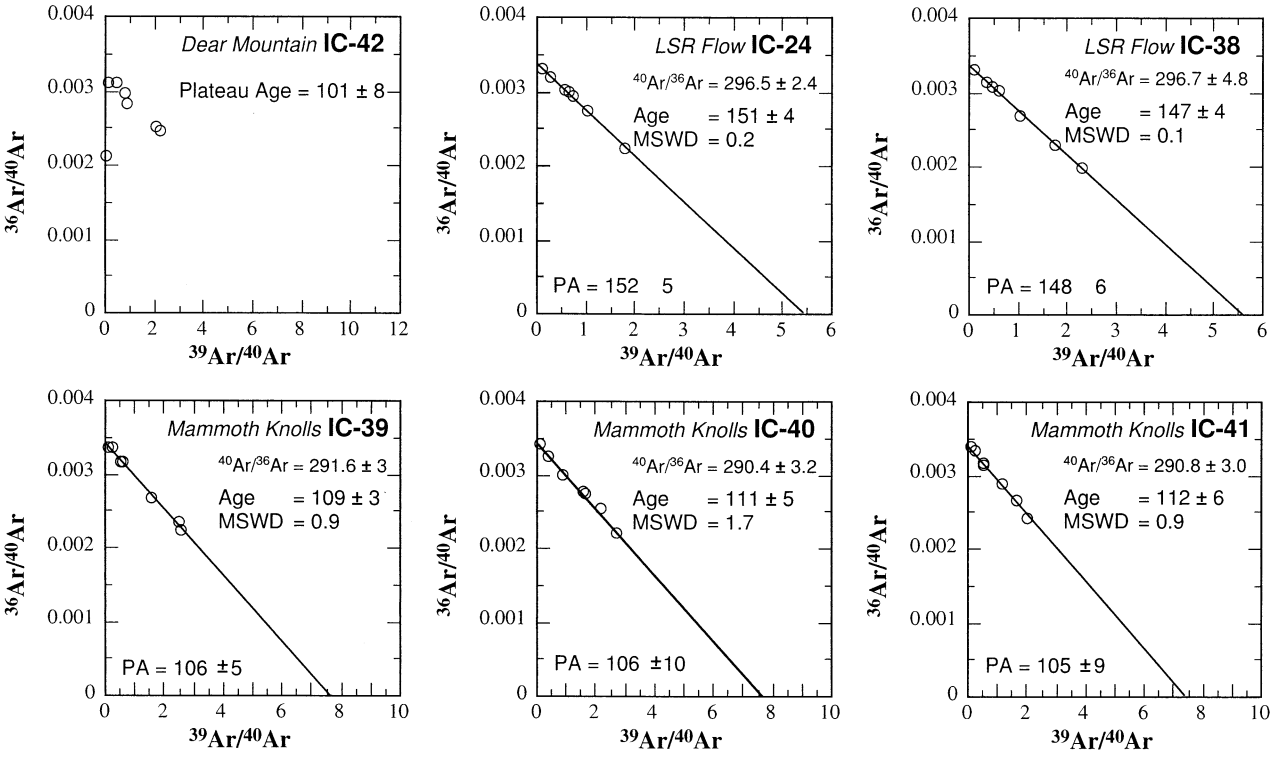

Fig. 4. Inverse isochron diagrams of incremental-heating and laser-fusion analyses of sanidines. Calculated ages in 10^3 yr. PA = plateau age.

switching with a ^{232}Th beam ~500,000 counts per second. This measurement yields the isotope dilution [Th]. The second data collection, at higher ion beam intensity (^{232}Th >200 mV), measured the ^{232}Th/^{229}Th and ^{232}Th/^{230}Th ratios statically by alternately switching the ^{229}Th signal and ^{230}Th signal onto the ion-counting system behind the RPQ filter (subsequently termed RPQ-SEM) and simultaneously collecting the ^{232}Th signal on one of two appropriately positioned Faraday collectors. This yields a drift independent ^{230}Th/^{229}Th ratio, and thus a [^{230}Th], and in combination with the first measurement a ^{230}Th/^{232}Th. ^{234}U/^{238}U and ^{233}U/^{238}U ratios were determined in a quadruple jump mode. In addition to static RPQ-SEM-Faraday ^{233}U/^{238}U and ^{234}U/^{238}U measurements, the ^{235}U/^{238}U ratio was measured twice, once as a static Faraday measurement to correct for instrumental mass fractionation and second as a RPQ-SEM-Faraday measurement to monitor ion counting yield. The mean value and reproducibility of the U950 standard were (^{234}U/^{238}U) = 0.974 and 0.2%. The Table Mountain Latite standard gave the following activity ratios: (^{238}U/^{232}Th) = 1.081, (^{230}Th/^{238}U) = 1.00, and (^{234}U/^{238}U) of 1.000 (calculated with decay constants used by Goldstein et al., 1989, and a revised λ(^{234}U) of Holden, 1989). Element concentrations determined by isotope dilution are better than 0.5%.

Eruption ages were determined by ^{40}Ar-^{39}Ar step-heating analysis of bulk sanidine separates (~50 mg with 200- to 400-μm grain size) according to the analytical procedure outlined in Wijbrans et al. (1995) and Heumann (1999). Regression of isochrons is based on the least-square method with 2σ error notation (McIntyre et al., 1966; York, 1969; Titterington and Halliday, 1979). All other errors cited in the text are at the 2σ level.

5. RESULTS

5.1. ^{40}Ar/^{39}Ar Ages

^{40}Ar/^{39}Ar age results obtained by incremental heating experiments of bulk sanidine separates from six samples are presented in Figure 4. The data (Heumann, 1999; and data available upon request) form well-defined isochrons (MSWD, 0.1 to 1.7). The isochrons yield initial ^{40}Ar/^{36}Ar ratios within error of the modern atmosphere (296). Ages of the three Mammoth Knolls are within analytical error and indicate eruption of the lavas at 110 ± 3 ka. In a previous study (Mankinen et al., 1986), sanidine analyses of the same domes yielded K-Ar ages within error of this study, although to poorer precision (110 ± 22 ka and 106 ± 8 ka for the northernmost and southern dome and 97 ± 12 ka for the middle dome; Fig. 1). The inverse isochron for the Deer Mountain Dome is less well constrained, and therefore the plateau age is reported here. The age of 101 ± 8 ka is within error of the previously reported K-Ar age; 115 ± 6 ka (Mankinen et al., 1986). The two samples from the large low-silica flow (IC-24, 38) have indistinguishable ages of 151 ± 4 ka and 147 ± 4 ka.

5.2. Rb-Sr Isotope Data

Rb-Sr isotope data for glasses and minerals from the Mammoth Knolls Domes, Deer Mountain Dome, and the LSR lava

Table 1. Rb-Sr and Pb isotope data for whole rocks, glass, and mineral separates.[a]

Sample[b]	Rb (ppm)	Sr (ppm)	$^{87}Rb/^{86}Sr$	$^{87}Sr/^{86}Sr$	$^{206}Pb/^{204}Pb$	$^{207}Pb/^{204}Pb$	$^{208}Pb/^{204}Pb$
			Mammoth Knolls Domes				
IC-39							
wr	168.4	46.02	10.59	0.706330 ± 15	19.178	15.690	38.932
gla	171.0	17.20	28.76	0.706387 ± 11	19.183	15.681	38.919
san	139.8	215.9	1.873	0.706284 ± 12	19.174	15.665	38.870
IC-40							
wr	172.7	38.67	12.92	0.706351 ± 13	19.178	15.689	38.928
gla	186.9	22.67	23.84	0.706364 ± 10	19.174	15.673	38.890
san	136.7	212.5	1.861	0.706304 ± 14	19.181	15.673	38.893
plag	79.89	221.4	1.044	0.706304 ± 11			
bio	818.9	27.67	85.62	0.707454 ± 11			
amph	50.71	26.64	1.520	0.706407 ± 10			
IC-41							
wr	162.5	57.87	8.123	0.706330 ± 13	19.182	15.687	38.930
gla	165.1	45.69	10.45	0.706322 ± 15	19.185	15.677	38.907
san	130.0	248.8	1.512	0.706284 ± 15	19.178	15.675	38.896
			Deer Mountain Dome				
IC-42							
wr	114.6	236.7	1.400	0.706294 ± 12	19.191	15.696	38.959
gla	137.5	139.5	2.850	0.706289 ± 12	19.190	15.675	38.901
san	171.4	501.3	0.9891	0.706300 ± 14	19.182	15.678	38.910
			LSR lava flow				
IC-24							
wr	136.3	134.5	2.931	0.706140 ± 12	19.175	15.682	38.921
gla	164.2	126.4	3.758	0.706169 ± 14	19.172	15.685	38.928
san	113.8	393.2	0.8371	0.706109 ± 13	19.198	15.693	38.965
IC-38							
wr	144.6	114.9	3.639	0.706127 ± 14	19.159	15.678	38.896
gla	168.5	107.0	4.554	0.706165 ± 13	19.185	15.687	38.941
san	130.0	478.1	0.7865	0.706145 ± 14	19.182	15.676	38.906

[a] Sr and Pb isotope compositions of whole rocks are from Heumann and Davies (1997) and listed for completeness.
[b] Wr = whole-rock; gla = glass; san = sanidine; plag = plagioclase; bio = biotite; amph = amphibole.

flow are presented in Table 1. When compared with their respective whole rocks (Heumann and Davies, 1997), low- and high-silica glasses have higher $^{87}Rb/^{86}Sr$ ratios, ranging from 2.8 for Deer Mountain to 28.7 in the Mammoth Knolls. This results from both higher Rb contents (137.5 to 186.9 ppm) in the glasses relative to whole rocks (114.6 to 172.7 ppm), and lower Sr contents down to 17.2 ppm. $^{87}Sr/^{86}Sr$ ratios of glasses vary between 0.70629 and 0.70638 in the dome samples and are 0.70616 in the LSR lava flow. The range of $^{87}Sr/^{86}Sr$ ratios in glasses is similar to whole-rock compositions, but individual glasses can be higher by $\sim 4 \times 10^{-5}$.

Both sanidine and plagioclase have lower $^{87}Sr/^{86}Sr$ ratios than host glasses ($\Delta^{87}Sr/^{86}Sr$ = 20 to 100), as would be expected for a low Rb/Sr phase. Sanidines from the Deer Mountain Dome have $^{87}Sr/^{86}Sr$ within error of the glass and whole rock, reflecting the comparatively modest (for these low-Sr rhyolites) Rb/Sr of this LSR. Strontium concentrations in the sanidine separates vary from 200 to 250 ppm in the Mammoth Knolls samples to 400 to 500 ppm in the LSRs from Deer Mountain and the LSR lava flow. The inferred sanidine–glass partition coefficients for Sr range from 3 to 15. These high Kd values are surpassed by plagioclase, which contains 613 ppm of Sr, and considering the 23 ppm in the glass, it indicates a mineral-melt partitioning ratio of 30 (IC-40). The values are in the range inferred and reported in previous studies (Blundy and Wood, 1991; Davies et al., 1994).

5.3. Pb Isotope Compositions

The Pb isotope ratios for glasses and feldspars listed in Table 1 are indistinguishable within the analytical precision. In a magmatic system that records significant temporal Pb isotope variations and hence implies open-system behavior (Heumann and Davies, 1997), these data provide strong evidence that sanidines are comagmatic phases.

5.4. U-Th Radionuclides

Table 2 lists U and Th concentrations and activity ratio data for whole rocks, glasses and minerals. The whole rocks show only minor isotopic disequilibrium ($(^{230}Th/^{238}U)$ = 0.97 to 1.03). Hand-picked glasses have U concentrations that are consistently higher than in the phenocryst-bearing whole rocks (Table 2). Thorium concentrations are lower in glasses than whole rocks in some LSRs but higher in HSR reaching a maximum of 20 ppm. ($^{230}Th/^{232}Th$) ratios of glasses are all >1 and higher than in the respective whole rocks (Fig. 6). The ($^{230}Th/^{238}U$) ratios of the glasses differ significantly from their host whole rocks and range from unity to 5.5% ^{238}U excess.

Minerals display a much greater extent of U-Th fractionation

Table 2. Concentration and activity data of U-series disequilibria.

Unit[a]	Sample[b]	U (ppm)	Th (ppm)	($^{238}U/^{232}Th$)	($^{230}Th/^{232}Th$)	($^{234}U/^{238}U$)
			Hornblende-Biotite Rhyolites (low-silica)			
Qmr3	IC-38					
	gla	4.44	13.28	1.014 ± 12	1.015 ± 4	1.001 ± 9
Qmr3	IC-24					
	wr	4.59	15.58	0.894 ± 1	0.915 ± 4	1.000 ± 3
	gla	4.74	13.39	1.072 ± 2	1.044 ± 5	1.004 ± 6
	san (1)	0.143	0.399	1.086 ± 2	1.005 ± 5	—
	san (2)	0.204	0.633	0.977 ± 4	0.937 ± 4	1.003 ± 10
	bio	0.683	1.848	1.121 ± 1	1.182 ± 7	—
	amph	0.545	2.836	0.583 ± 1	0.675 ± 3	1.004 ± 6
	zirc	250.7	134.4	5.657 ± 5	4.921 ± 30	1.001 ± 5
Qmr3	IC-42					
	wr	3.57	12.23	0.885 ± 1	0.913 ± 3	1.002 ± 3
	gla	4.71	13.94	1.024 ± 2	1.033 ± 4	1.004 ± 7
	san	0.0305	0.0858	1.078 ± 2	1.138 ± 17	1.006 ± 9
	bio	0.464	1.60	0.878 ± 1	0.964 ± 13	1.016 ± 8
	amph	0.335	3.31	0.307 ± 1	0.453 ± 6	1.007 ± 7
	zirc	118.6	87.69	4.100 ± 8	3.812 ± 20	1.003 ± 5
			Mammoth Knolls Rhyolites (high-silica)			
Qmrm	IC-41					
	wr	6.15	18.13	1.029 ± 1	1.020 ± 4	1.000 ± 2
	gla	6.57	17.83	1.117 ± 1	1.066 ± 6	1.005 ± 5
Qmrm	IC-40					
	wr	6.57	18.46	1.079 ± 1	1.046 ± 3	1.003 ± 3
	gla	7.09	18.72	1.149 ± 2	1.090 ± 5	0.999 ± 6
	bio	0.72	2.61	0.834 ± 1	1.201 ± 2	1.021 ± 8
	zirc	509.2	367.9	4.195 ± 7	3.296 ± 11	1.004 ± 10
Qmrm	IC-39					
	wr	6.51	18.61	1.060 ± 1	1.025 ± 5	1.000 ± 1
	gla	7.58	20.03	1.147 ± 2	1.084 ± 3	0.998 ± 3
	zirc	633.4	475.0	4.043 ± 7	3.210 ± 16	1.000 ± 5

[a] From Bailey (1989).
[b] Wr = whole rock; gla = glass; san = sanidine; bio = biotite; amph = amphibole; zirc = zircon.

and consequently deviation from ^{230}Th-^{238}U equilibrium. Zircons have the most extreme U/Th ratios, with U concentrations between 118 to 633 ppm and Th concentrations ranging from 87 to 475 ppm. Other mineral phases have much lower U-Th contents than the glasses. ($^{230}Th/^{232}Th$) ratios vary from 4.9 in zircons to 0.45 in amphiboles, and the degree of isotopic disequilibrium ranges from 7 to 22% ^{238}U enrichment in zircons to between 44 and 75% ^{230}Th enrichment in amphiboles. ($^{234}U/^{238}U$) ratios are within error of unity, except two biotites that have ($^{234}U/^{238}U$) marginally greater than unity.

6. DISCUSSION

6.1. Rb-Sr Isochron Ages

Heumann and Davies (1997) established that the whole-rock Rb-Sr isotope compositions of the Deer Mountain and Mammoth Knolls rhyolites fall along a linear trend, corresponding to an age of 277 ± 124 ka, which is apparently older than the $^{40}Ar/^{39}Ar$ eruption ages of the domes (~110 ka). The corresponding glass analyses for these samples in this study confirm the preeruptive age information, indicating a Rb-Sr isochron of 257 ± 39 ka, which is more significantly distinct from the ^{40}Ar-^{39}Ar eruption age (Fig. 5). Additionally, the combined data set of whole rocks and glasses yields an indistinguishable age of 229 ± 63 ka (data not shown). The glasses, as melt compositions without contributions from minerals with potentially different histories, clearly provide a less scattered isochron and thus a more precise Rb-Sr age for these rocks. To interpret the array in Figure 5 as a preeruptive magma formation age, however, it must be shown that other conceivable processes did not cause the linear trend.

Assimilation of country rock has been advocated to explain large $^{87}Sr/^{86}Sr$ variations of precaldera rhyolites (Knesel and Davidson, 1997). An assimilation process can be ruled out for

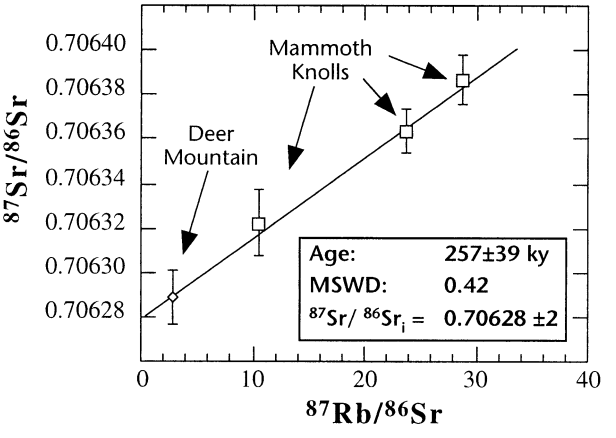

Fig. 5. Rb-Sr isochron diagram for glasses of the three Mammoth Knolls Domes and the Deer Mountain Dome. Apparent isochron age is ~150 ky older than eruption age. See text for discussion.

Table 3. Rayleigh fractional crystallization model for high-silica rhyolites of Mammoth Knolls.[a]

Fractionation	Sum of crystals removed	Rb (ppm)	Sr (ppm)	$^{87}Rb/^{86}Sr$
IC-41 ($^{87}Sr/^{86}Sr = 0.706322$)				
Original melt	0	165.1	45.70	10.45
Step 1 to produce IC-40				
Sanidine	5.8%	161.5	19.71	23.61
Plagioclase	2.8%	165.8	20.05	23.93
Step 2 to produce IC-39				
Sanidine	7.2%	160.6	16.05	28.95
Plagioclase	3.4%	166.0	16.76	28.66

[a] Partition coefficients (IC-40): sanidine $Kd_{Rb} = 1.37$, $Kd_{Sr} = 15$; plagioclase $Kd_{Rb} = 0.84$, $Kd_{Sr} = 30$.

the postcaldera rhyolites that define the Rb-Sr isochron. This is because potential contaminants have completely different Sr-Pb-Nd isotope and trace element compositions (Heumann and Davies, 1997), yet the rocks that define the isochron in Figure 5 have indistinguishable Pb isotope compositions that plot on the well-defined temporal trend of postcaldera rhyolites (Fig. 2).

The glasses with the highest $^{87}Sr/^{86}Sr$ ratio have consistently the lowest Sr concentrations (Table 1) and are chemically more evolved than other rhyolites. Mixing of isotopically contrasting melts within the Long Valley system could potentially produce positive or negative correlations between $^{87}Sr/^{86}Sr$ and $^{87}Rb/^{86}Sr$ ratios. Although negative correlation of $^{87}Sr/^{86}Sr$ ratio and Sr concentration (1/Sr; data not shown) can only be ascribed to a mixing process, a positive correlation, as defined by these data, can be due to either magma mixing or to Sr depletion by fractional crystallization of feldspars with subsequent aging of the melts. To explain the linear trend in Figure 5, two-component mixing would require an end member with a relatively high Sr concentration and a low $^{87}Sr/^{86}Sr$ ratio and an end member with a low Sr concentration and a higher $^{87}Sr/^{86}Sr$ ratio. As explained above, assimilation of local country rocks (e.g., Duffield et al., 1995; Knesel et al., 1999) does not seem to account for this second component (see detailed discussion in Davies and Halliday, 1998). Preferential assimilation of biotite breakdown products has been proposed as a possible mechanism (Knesel and Davidson, 1997), but it is hard to see how such a physical mechanism could operate in a relatively low-temperature magmatic system the size of Long Valley, which has biotite on the liquidus. Significantly, the Sr isotope and elemental characteristics of these components are the same as expected from fractional crystallization. In contrast to many mafic and intermediate rocks, Sr is a highly compatible element in rhyolites (e.g., Halliday et al., 1991), as demonstrated by the large partition coefficients of Sr into feldspars (Table 1). Relatively small degrees of feldspar fractionation can therefore cause a range of Rb/Sr ratios in the magma, which, upon prolonged magma storage and decay of ^{87}Rb, will produce a linear array with a constant initial $^{87}Sr/^{86}Sr$ ratio of $\sim$0.70630. A quantification of the amount of feldspar fractionation required to create the observed variation of $^{87}Rb/^{86}Sr$ in the Mammoth Knolls samples is presented in Table 3. The maximum difference in $^{87}Rb/^{86}Sr$ between samples IC-41 and IC-39 is explained by $\sim$7% sanidine fractionation or $\sim$3% plagioclase fractionation. We conclude that the Rb-Sr data are readily explained by small amounts of sanidine and plagioclase fractionation and reject mixing scenarios, which require an ad hoc explanation.

If Rb-Sr fractionation was controlled by a feldspar-rich mineral assemblage and the melt remained a closed system thereafter, then feldspar–glass pairs should give the age of this event. The Rb-Sr age relationships of whole rocks, glasses, and feldspars are presented in Table 4. For the HSR samples IC-39 and IC-40, the feldspar–glass ages are within error of the glass isochron of 257 $\pm$ 39 ka and have identical initial Sr isotope ratios. The relatively low Rb/Sr ratios of the LSR yield errors larger than HSR mineral–glass ages. The glass–glass and mineral–glass ages, however, overlap and therefore provide strong evidence for preeruptive Rb-Sr fractionation in these rhyolites.

The analyzed mafic phases (biotite and amphibole) analyzed for sample IC-40, however, have Sr isotope signatures in disequilibrium with the host rhyolitic melt composition. None of the glasses have $^{87}Sr/^{86}Sr$ ratios $>$0.70635, and therefore the values obtained for the mafic phases ($>$0.7064) possibly indicate contributions of xenocrystic material or open-system behavior of Rb. Selective contamination with xenocrystic biotite crystals must be limited so as not to disturb the temporal isotope variations in the rocks. Contamination must also be restricted to events occurring shortly before eruption because diffusive processes are comparatively fast for biotite, forcing isotopic reequilibration with the melt within a few months (Freer, 1981; Giletti, 1990). Similar conclusions on the isotope compositions of biotites have been drawn from studies on Long Valley precaldera rhyolites (Christensen and DePaolo, 1993; Davies et al., 1994; Davies and Halliday, 1998). It is also noteworthy that the biotites display minor ($^{234}U/^{238}U$) disequilibrium, suggestive of a more complex history. Alternatively,

Table 4. Rb-Sr age relationships (ky) between whole rock, glasses, and minerals.

Sample	Isochron[a]	$^{87}Rb/^{86}Sr$ age	MSWD	$^{87}Sr/^{86}Sr_i$
IC-39, 40, 41, 42	wr	277 $\pm$ 124	0.62	0.70630 $\pm$ 1
IC-39, 40, 41, 42	glasses	257 $\pm$ 39	0.42	0.70628 $\pm$ 1
IC-39, 40, 41, 42	glass, wr	229 $\pm$ 63	2.37	0.70629 $\pm$ 2
IC-39, 40, 41, 42	glass, wr, fsp	225 $\pm$ 51	3.26	0.70629 $\pm$ 1
IC-40	glass, san, plag	188 $\pm$ 41	0.05	0.70630 $\pm$ 1
IC-40	glass, san	192 $\pm$ 77	—	0.70630 $\pm$ 1
IC-39	glass, san	270 $\pm$ 60	—	0.70628 $\pm$ 1

[a] Wr = whole rock; fsp = sanidine and plagioclase feldspars; san = sanidines; plag = plagioclase.

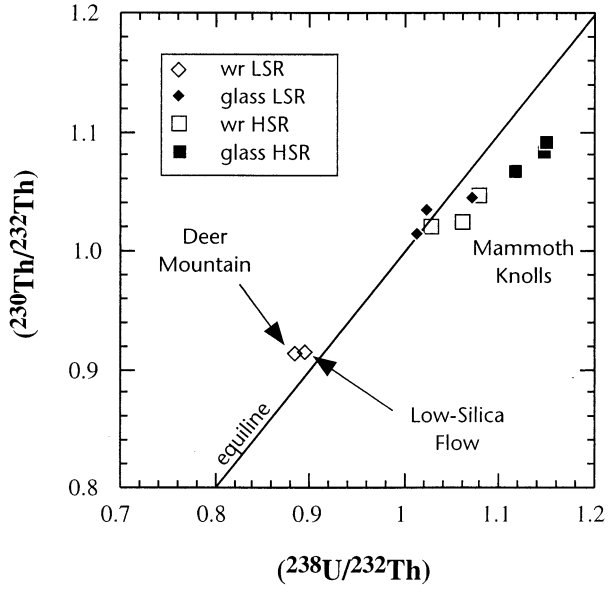

Fig. 6. (^{232}Th/^{230}Th) vs. (^{238}U/^{232}Th) activity ratio diagram for whole rocks and selected glasses of Long Valley postcaldera rhyolites. Symbols are larger than error bars. Note that glasses have consistently lower (^{230}Th/^{238}U) than the respective whole rocks, which plot to the left of the equiline for LSR and to the right for HSR.

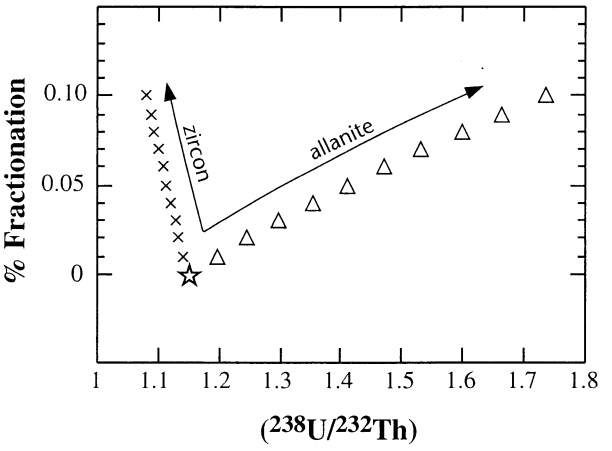

Fig. 7. Effect of accessory mineral fractionation of allanite and zircon on the U/Th ratio of melt. Star = starting compositions of the melt. Calculations are based on Rayleigh fractionation law assuming U and Th partition coefficients deduced from isotope dilution analyses, microprobe analyses (allanite), and U/Th ratios of allanites from the literature (Barth et al., 1994). To change the (^{238}U/^{232}Th) of a melt to the same extent requires 10 times more zircon than allanite fractionation. This demonstrates the dominating role of allanite over zircon in fractionating Th from U in the residual melt.

the mobility of Rb and Sr in hydrous phases such as biotites and amphiboles could be high enough during long-term magma storage that Rb-Sr systematics are disrupted in these minerals. Nevertheless, the results presented in this section palpably demonstrate the dominant role of feldspar fractionation in creating the observed Rb-Sr variation in the melts. The Rb-Sr age information therefore appears to support the hypothesis that rhyolite formation precedes eruption by ~150 ky, as proposed by Heumann and Davies (1997) and Reid et al. (1997).

6.2. ^{230}Th-^{238}U Disequilibrium Data

Accessory phases are known to have a major control on trace element partitioning in HSR (Arth, 1976; Mahood and Hildreth, 1983; Nash and Crecraft, 1985; Cameron and Cameron, 1986; Michael, 1988). Zircons analyzed in this study have the commonly observed enrichment of U over Th (Table 2), but inferred partition coefficients are highly variable, with Kd_U = 25 to 53, Kd_{Th} = 6 to 10 in the LSRs, and Kd_U = 70 to 83, Kd_{Th} = 19 to 23 in the HSRs. The whole-rock compositions, however, show lower U/Th than the glasses (Fig. 6), and the bulk phenocryst populations must be enriched in Th relative to U compared with the glass. This indicates that a phase other than zircon and with a high Th/U ratio dominates the U-series systematics of the rhyolites.

Heumann and Davies (1997) demonstrated that variations in rare earth element and high field strength element contents of the postcaldera rhyolites at Long Valley required fractionation of a combination of zircon, apatite, and allanite, which are cogenetic phases. Of these phases, allanite causes the greatest Th/U fractionation (e.g., Hildreth, 1979; Mahood and Hildreth, 1983) and can have exceedingly high Th concentrations (up to 12,000 ppm) and Th/U ratios between 80 to 150 (e.g., Barth et al., 1989, 1994). Electron microprobe analyses indicate that allanites from the Long Valley rhyolites have Th concentrations that range from 3000 to 12,000 ppm. Hence, even the scarce occurrence of ~200-μm allanite crystals (Fig. 3) is consistent with allanite as the major Th fractionating phase. For example, to affect the (^{238}U/^{232}Th) of rhyolitic melts to the same extent requires 10 times more zircon fractionation (by mass) than allanite (Fig. 7) and even greater amounts of apatite. Crystallization of allanite with exceedingly high Th/U ratios is therefore considered the major control of the U-Th evolution during fractional crystallization of this magmatic system.

6.3. ^{238}U-^{230}Th Internal Isochrons

Internal, or mineral, ^{230}Th-^{238}U isochrons of four rocks are presented in Figure 8. Minerals from the LSR IC-42 (Deer Mountain Dome) exhibit a well-defined linear trend corresponding to an age of 235.6 ± 1.2 ka with $(^{230}\text{Th}/^{232}\text{Th})_i$ = 1.596 ± 8. This age is 135 ky older than the eruption age (Δt = 135 ky) and is in the range of the preeruptive ages from ion-probe U-Th measurements of individual zircons from this dome (Reid et al., 1997; see below). The melt phase (glass), however, plots below this linear array on the equiline with (^{238}U/^{232}Th) ~1, and the whole rock lies below the mineral array on a mixing line between the glass and the amphibole, the latter having the highest Th/U ratio. The glass–amphibole age is significantly younger (180 ± 2 ka) than the glass–zircon age (253.7 ± 3.5 ka) but is still significantly older than the 101-ka eruption age (Table 5). Biotite and sanidine plot directly above the whole-rock and glass compositions so that these phases do not yield mineral–glass ages. The well-defined mineral isochron therefore cannot be interpreted as the crystallization age of the bulk mineral population. Similar relationships between glasses and minerals exist for the other samples, although they do not define good linear relationships. In all cases, zircon–

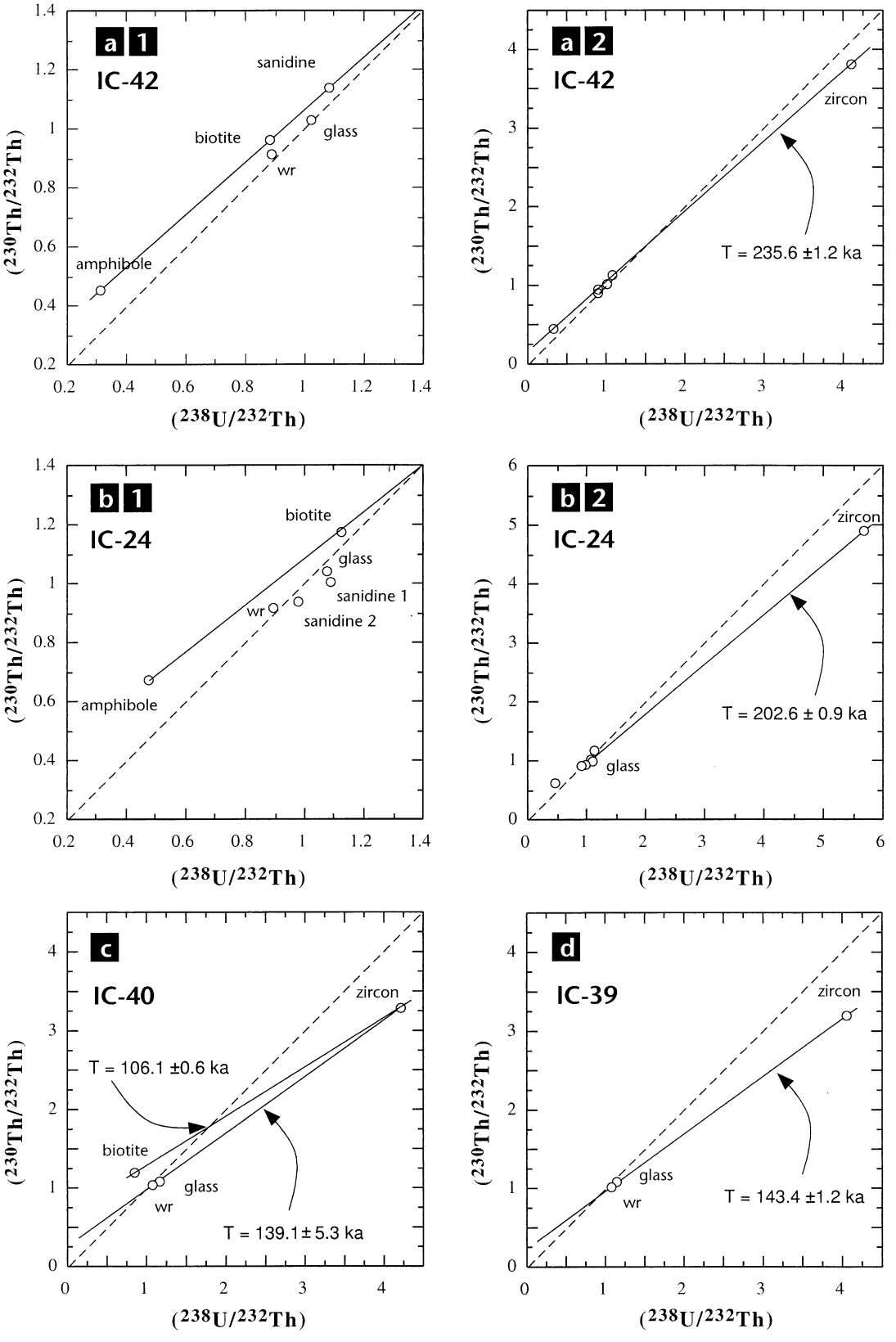

Fig. 8. ^{230}Th-^{238}U isochrons for whole rocks, glasses, and minerals from postcaldera rhyolites of the Long Valley system erupted between 110 and 150 ky. (a1, b1) Enlarged areas of diagrams (a2) and (b2), which also include the zircons with their much higher U/Th ratios. Dashed lines = equilines. Lines for age reference were calculated with a least-square linear regression technique (York, 1969). Error bars are all smaller than symbol size.

Table 5. ($^{230}Th/^{238}U$) age relationships (ky) between minerals, glasses, and whole rocks.

Sample	$^{40}Ar/^{39}Ar$ age	Isochron[a]	$^{230}Th/^{238}U$ age	$(^{230}Th/^{232}Th)_i$	Δ Age
IC-42	101 ± 8	san-bio-amph-zircon	235.6 ± 1.2	1.596 ± 0.008	135 ± 3
		zircon-glass-wr	251.2 ± 1.4	1.154 ± 0.008	150 ± 3
		zircon-glass	253.7 ± 3.5	1.121 ± 0.020	153 ± 5
		amph-glass	179.8 ± 2.0	1.073 ± 0.015	79 ± 4
IC-24	151 ± 4	wr-amph-zircon	175.6 ± 12.9	1.840 ± 0.006	25 ± 13
		zircon-glass	202.6 ± 0.9	0.891 ± 0.020	52 ± 3.7
		amph-glass	152.6 ± 2.0	0.953 ± 0.020	0
IC-40	111 ± 5	wr-glass-zircon	139.1 ± 5.3	0.952 ± 0.008	28 ± 6
		zircon-glass	139.7 ± 0.8	0.936 ± 0.020	29 ± 3
IC-39	109 ± 3	wr-glass-zircon	143.4 ± 1.2	0.914 ± 0.011	34 ± 2
		zircon-glass	143.8 ± 0.9	0.915 ± 0.020	35 ± 2

[a] Wr = whole-rock; gla = glass; san = sanidine; plag = plagioclase; bio = biotite; amph = amphibole.

glass ages are significantly older than the eruption ages (Δt = 29 to 52 ky; Table 5). The amphibole–glass age of LSR sample IC-24 (153 ± 2 ka) is within error of the eruption age (151 ± 2 ka) and thus is clearly younger than its glass–zircon age. The relatively high Th contents and low U/Th ratios of the amphibole, as for IC-42, imply that it contains a Th-rich minor phase (allanite) that dominates the U-Th systematics of the mineral separate. Biotites in samples IC-24 and IC-40 again plot above the whole rock and glass on an equiline diagram; the sanidines of IC-24 plot below the glass.

Similar mineral–glass ^{238}U-^{230}Th relationships to that shown by the postcaldera rhyolites were reported in the studies that led to the introduction of the ^{230}Th-^{238}U equiline diagram (Taddeucci et al., 1967; Allègre, 1968). The apparent discrepancy between minerals and glass was attributed to early crystallization of the mineral phases in the magma chamber, followed by partial melting of the same minerals during the eruption process. In such a scenario, it is, however, impossible to maintain the mineral isochron because partial melting would inevitably alter the U/Th ratios of the minerals. The postcaldera rhyolites under study retain no obvious petrological evidence of remelting older crystalline material or chemical mixing. Modeling of the long-term (700 ky) open-system evolution of the Long Valley system, which is characterized by a coupled, temporal decrease in Pb and Sr isotope ratios, shows that the recharge magmas must have dacitic to rhyolitic compositions that are isotopically different to older Long Valley rhyolites (Heumann, 1999; and data available upon request). Thus, remelting of earlier crystallized material from the Long Valley system does not appear to be a tenable interpretation. Although remelting scenarios might offer viable explanations for other, less differentiated magmatic systems (e.g., Crater Lake caldera; Bacon et al., 2000), the combined Sr-Pb and U-Th data of the rhyolites in this study are most simply interpreted in the context of magma recharge and mineral crystallization. Thus, we interpret the preeruptive zircon and allanite ages as geologically significant; these data indicate protracted postcrystallization residence times in the magma chamber, further strengthening the arguments from Rb-Sr systematics.

The line defined by the mineral data from IC-42 in a ^{230}Th-^{238}U equiline diagram (Fig. 8a) only yields a true age if there was rapid, contemporaneous crystallization of two accessory phases with opposite U-Th partitioning (e.g., zircon-allanite). Because the melt phase (glass) does not lie on the mixing line defined by the minerals, this cannot be the case. The simplest scenario to explain the glass plotting below the mineral trend is that the two accessory phases crystallized at different times, and in this instance, only the mineral–glass age of the last formed mineral provides true age information. Thus, there is no absolute age significance to the especially well defined linear correlation of the minerals from IC-42 (Fig. 8a). The topology of data points, however, still provides important age information. For example, the U-Th isotope systematics of amphibole is likely a mixture of amphibole, zircon, and allanite. Although dominated by allanite, pure allanite should have a much lower U/Th, and thus the amphibole–glass age represents a lower estimate of the time of allanite crystallization in sample IC-42 (180 ± 2 ka). Extrapolation of the linear trend in Figure 8a1 to $(^{238}U/^{232}Th) = 0$ gives a maximum age of allanite crystallization (193 ± 2 ka). The time of allanite crystallization is therefore constrained to 187 ± 9 ka, which is ~70 ky after zircon and feldspar crystallization.

The probable evolution of the U-Th fractionation in sample IC-42 is presented schematically in Figure 9. The two-stage fractionation model includes initial zircon and later allanite crystallization. In the model, we assume that the initial melt composition is in secular equilibrium, but this is not a prerequisite of the model. In addition, we assume that all the mineral phases are cogenetic. This conclusion is justified by the whole rock, glass, and sanidine being in Pb isotope equilibrium (Table 1). At time t_1, zircon crystallizes, causing the remaining melt composition to have a small ^{230}Th excess (G_1; Fig. 9a). With time, the melt returns toward secular equilibrium (Fig. 9b), but at time t_2, allanite crystallization causes the melt to inherit a significant ^{238}U excess (Fig. 9c). Subsequently, there is no further crystallization of major U and Th partitioning phases. Consequently, mixing zircon and allanite populations will result in a well-defined linear array (e.g., IC-42; Figs. 8a, 9d), and the mineral and glass will form an obtuse-angled triangle. The mineral array defined by minerals from IC-42 consequently has no true age significance. The only true age can be obtained from the last phases to crystallize. In the case of sample IC-42, this would be the allanite concentrated in the amphibole.

The U-Th isotope systematics of samples IC-24 and IC-40 are significantly more complex than those of IC-42, with the minerals not defining a single mixing array. The glass–amphibole age from LSR sample IC-24 (153 ± 3 ka) is within error of the eruption age, whereas the zircon–glass age is 50 ky

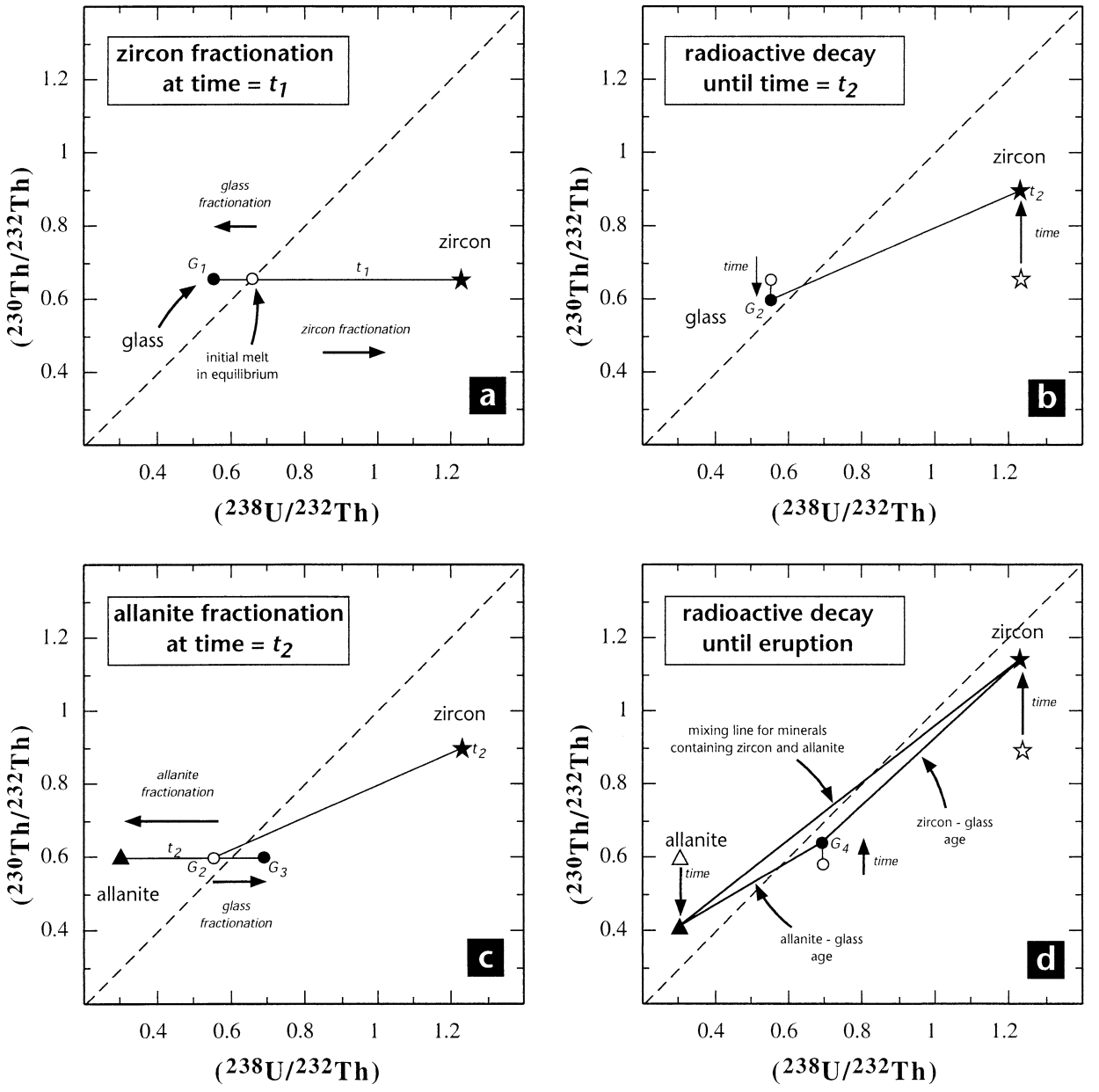

Fig. 9. Schematic ($^{232}Th/^{230}Th$) vs. ($^{238}U/^{232}Th$) activity ratio diagram for the Long Valley western moat rhyolites. (a) The initial melt, in secular equilibrium, fractionates zircon at time t_1 and melt composition consequently moves to the left of the equiline G_1. Radioactive aging results in the glass and the zircon moving toward the equiline (b, G_1–G_2). (c) Allanite fractionation at time t_2 causes an increase of the U/Th ratio in the remaining melt and consequently a shift to the right (G_3). (d) Further aging until today. Accessory phases and melt will not define a linear relationship but a triangle with an obtuse angle. Only the last fractionation event (t_2) will give valid mineral–glass ages (allanite-G_4); zircon crystals that crystallized early during magmatic evolution will not be in isotopic equilibrium with G_4. Note that if there is later crystallization of a second generation of zircon, for example, it will plot below the filled star in (d). Zircons formed at the time of eruption would have $^{230}Th/^{232}Th$ identical to the glass. Minerals from sample IC-42 define a linear array that indicates that the zircon and allanite populations were formed in single events.

older. Sanidines from sample IC-24 have up to 8% ^{238}U excess and plot significantly below both the zircon–amphibole mixing line and the glass and whole-rock compositions. They define a two-point line with a slope equal to 106 ± 10 ka, ~50 ky younger than the eruption age of the host rock. This relationship may suggest that the sanidines are not cogenetic with the remainder of the rock. Such a conclusion is at odds with the Sr and Pb isotope equilibrium between the minerals and host glass (Table 1). As with sample IC-42, the explanation of the U-Th disequilibria probably lies in the crystallization history of the minor phases. The ^{238}U excess of the sanidine can best be explained as a consequence of zircon inclusions. The sanidines plot below a line between zircon and glass/whole rock, implying that the analyzed zircon population (large, euhedral) are not

those responsible for the ^{238}U excesses of the sanidines. In addition, the posteruption age ("negative age") of the sanidine pair and their position below the glass on the equiline diagram require that these phases contain a mixture of allanite and zircons younger than the large euhedral population. Petrographic observations establish that there are several generations of minor phases (Fig. 3), and two or more generations of zircon fractionation can readily explain the U-Th isotope systematics of these rocks.

It is notable that biotite separates all have U-Th compositions that lie above the glass and whole-rock compositions. This implies that, as with the sanidine in sample IC-42, biotite contains populations of both accessory phases. However, the biotites were also anomalous in the Rb-Sr system, and their minor $^{234}U/^{238}U$ disequilibrium raises the possibility that the biotites may be xenocrystic or show significant open-system behavior. Although accessory phases have been seen as inclusions in both biotite and sanidine, they are also commonly attached to the margin of the major phenocryst phases and even to large zircons (e.g., Fig. 3c). It is therefore impossible to conclude unambiguously from the U-Th mixing relationship of IC-42 whether the major phenocryst phases crystallized before or after the accessory phases. In this case, we must rely on other geochemical information, such as the Rb-Sr systematics.

We conclude that the linear U-Th relationships, as shown by minerals from the postcaldera rhyolites, are most likely a consequence of a mixing process involving accessory minerals that control U-Th fractionation. The U-Th disequilibrium data presented in this study are best explained by a semiquantitative model, with crystallization of two accessory mineral phases at different times. In addition, the coherent mixing relationship defined by the minerals from IC-42 requires that, for this sample at least, crystallization of minor phases occurred up to 150 ky before magma eruption and that crystallization was in discrete and rapid events.

6.4. Crystallization History of Accessory Phases

Accessory minerals such as zircon, apatite, or allanite contain Zr, P, or rare earth elements as essential structural constituents (Sun and Hanson, 1975) in their crystal structure and crystallization first requires saturation of these elements in the melt. The occurrence of all these accessory phases in both LSRs and HSRs indicates early melt saturation in essential structural constituents (at ~70 wt% SiO_2). Petrographic criteria, such as the contrasting crystal sizes and shapes for zircons, do not unequivocally allow the determination of the crystallization sequence of the accessory minerals. The close spatial association of some accessories as glomerophyric clots of zircon, allanite, apatite, and magnetite indicates mutual influence during nucleation. The smallest accessory minerals occur as euhedral grains as inclusions in or on the surfaces of the major phenocryst grains. These occurrences alone are not necessarily proof of the early appearance of accessory phases on the liquidus. Crystallization of accessory phases can also result from local saturation adjacent to, and therefore contemporaneous with, the major phenocryst phases (Bacon, 1989).

Above, we established that fractional crystallization is not always a simple two-stage process, as inferred for IC-42. The well-defined mixing relationship of sample IC-42 establishes that at least in this case, crystallization of allanite and euhedral zircons must have occurred within the time resolution of the mixing line, —that is, ±1.2 ky. In contrast, the isotopic heterogeneity of samples such as IC-24 implies accessory mineral formation was more protracted or episodic. Multiple crystallization events (e.g., Charlier and Zellmer, 2000) are not readily detectable by analysis of mineral composites. The large euhedral zircons, however, always define the oldest mineral–glass ages (Table 5). Therefore, these zircons apparently reflect early onset of crystallization during magmatic evolution. Extended or multiple periods of minor phase formation would form mineral populations with different ($^{230}Th/^{232}Th$) ratios lying in near vertical arrays (between the star symbols in Figure 9d). There is, however, evidence for younger crystallization ages of zircons in some rocks from this study and in the previous ^{238}U-series study by Reid et al. (1997), which determined individual zircon ages from the Deer Mountain Dome (100 ka) and the southernmost Inyo Dome (~0.6 ka) by ion microprobe. The impetus for that study arose from earlier observations that noted the remarkable petrographic resemblance and close spatial association of the lavas from both domes (Bailey et al., 1976; Sampson and Cameron, 1987). Although the eruption ages of the lavas differ by 100 ky, the majority of zircons apparently shared a common crystallization age of ~230 ka. The reported zircon model ages, calculated with the ($^{230}Th/^{232}Th$) of the whole rock as the initial ratio, are similar to the ages obtained from our study of the Deer Mountain sample IC-42 (Table 5).

The TIMS measurements yield a much better precision than the ion microprobe approach. Importantly, however, single spot analysis by ion microprobe potentially allows identification of a large range in U/Th ratios and possibly different age generations of zircons (e.g., Reid et al., 1997; Brown and Fletcher, 1999; Bacon et al., 2000; Lowenstern et al., 2000; Reid and Coath, 2000) but requires a large number of measurements to overcome the large uncertainties of model ages on the basis of single-grain analysis by ion probe. The largest zircons from the low-silica samples (IC-24, IC-42) in our study overlap a proportion of the Reid et al. (1997) data with crystallization ages >200 ka, whereas the zircons from the HSR are comparable to a group of younger zircon grains, identified by the ion microprobe (140 to 150 ky). A small proportion of the zircons from the ion probe study is also shown to have ages close to the eruption age of the rock. This observation is consistent with our conclusion from sample IC-24 that some rocks must have undergone protracted periods, several periods, or both of minor phase crystallization. The microprobe approach is ideal for determining if the minerals have complex crystallization histories. Individual grain or population analysis by TIMS provides the most precise age information and is therefore the best approach to determine absolute timing and rates of crystallization.

6.5. Physical Evolution of Magma Reservoir

Accessory mineral fractionation occurred in the LSR (IC-42) up to 150 ky and in the HSR ~35 ky before eruption. The older preeruptive U-Th age is identical to the Rb-Sr results that we interpret to reflect the onset of feldspar fractionation at 250 ka. These ages place stringent limits on the dynamic evolution of

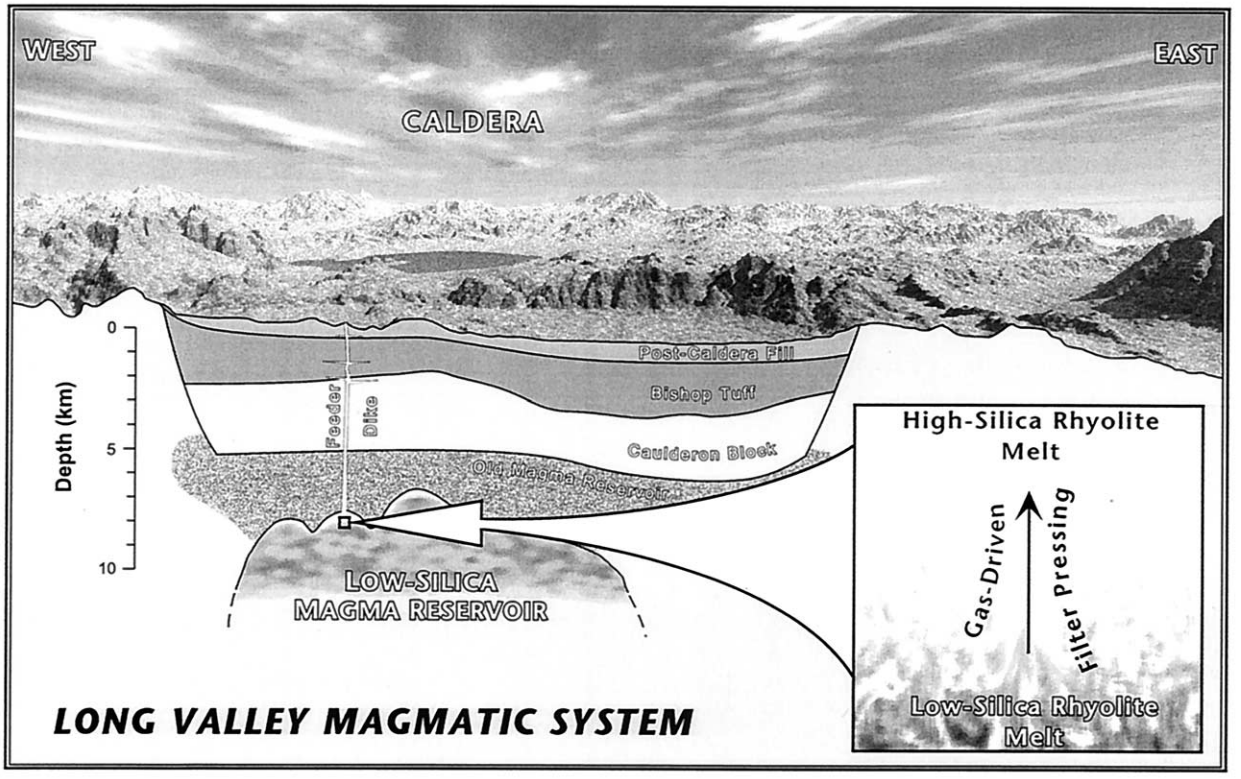

Fig. 10. Schematic model of the Long Valley magma system at ~200 ka. The major low-silica magma volume is well mixed and represents an open-system magma reservoir, periodically fed from below (Heumann and Davies, 1997; Heumann, 1999). Filter pressing, driven by the exsolution of gas, forces highly differentiated interstitial liquids from the dominant magma volume, forming HSR. Simultaneously, the exsolution of gas inflates cupolas in the upper reaches of the reservoir, where the high-silica melts accumulate and are stored for up to 150 ky before eruption.

the magmatic reservoir. The solubility of zircon crystals in felsic magmas is a function of melt temperature and composition (Watson and Harrison, 1983). Calculated zircon saturation temperatures are well below 800°C (Heumann, 1999) and indicate a clear temperature decrease with increasing fractionation from LSR to HSR. These temperatures confirm results obtained from Fe-Ti oxides (Vogel et al., 1989). Currently, no solubility data exist for allanite, but by analogy to monazite, we predict allanite crystallization temperatures would be ~50°C lower than zircon (Montel, 1993). From the zircon solubility models, it is possible to assess how slight temperature variations would change the stability of minor phases in the rhyolitic melt (Harrison and Watson, 1983). Solution kinetics suggest that 50-μm zircon grains would be totally dissolved in tens of years if temperature were raised by as little as 50°C (Harrison and Watson, 1984). The majority of zircon phenocrysts have euhedral crystal shapes and appear to be in chemical equilibrium with the melt (Fig. 3). Smooth crystal edges of a very minor proportion of the zircon population (<0.5% of the 10-μm grains) may document small changes in the temperature conditions. The euhedral nature of the majority of minor phases implies that temperature changes must have been limited to significantly less than 50°C. Together with preeruption ages of 80 ky for allanites from IC-42, these data constrain the thermal evolution of the magma body. After a feldspar fractionation event and zircon saturation at ~250 ka (~790°C), the magma cooled to ~740°C by 180 ka (time of allanite crystallization), and there is no evidence that temperature increased before eruption as a crystal-poor lava at 101 ka. The implied cooling rate of this magma is therefore on the order of 7×10^{-4} °C /a between zircon and allanite crystallization. Melting experiments imply that the solidus of magmas of this composition is 700°C (Bohlen et al., 1995). Therefore, the integrated cooling rate over the entire preeruptive history is less than $\sim 6.4 \times 10^{-4}$ °C/a because the magma did not reach the solidus. HSR lavas record similar slow cooling. Zircons of IC-39 formed at 725°C ~35 ky before eruption of the lava. Solidus estimates for the HSR are ~680°C, which imply integrated cooling rates significantly below 1×10^{-3} °C /a.

The long inferred preeruptive storage times and slow cooling rates imply that the thermal budget of the magmatic reservoir must have been buffered by either influx of compositionally similar magma or by thermal support from an underlying, much larger and less evolved melt volume. The constantly decreasing $^{87}Sr/^{86}Sr$ of the postcaldera rhyolites establishes that the Long Valley system was sustained by melt addition (Heumann and Davies, 1997) over a timescale of ~700 ky. The relatively small melt volumes representing Mammoth Knolls, Deer Mountain, and the LSR flow could have been erupted from the roof areas of the system where magma was effectively separated from major convection and mixing. Feldspar fractionation at ~250 ka (Rb-Sr ages) and the succession of zircon crystal-

lization ages (U-Th) from ~250 ka (Deer Mountain), ~200 ka (LSR flow), and ~140 ka (Mammoth Knolls) imply that the upper parts of the magma chamber underwent recurrent periods of magma undercooling and accessory phase crystallization. The amount of feldspar fractionation required to produce the spread of Rb/Sr ratios in the glasses quantitatively outweighs the minor effects of accessory mineral crystallization on bulk melt compositions. The last major chemical differentiation registered by the magmas is therefore the 250-ka event recorded by Rb-Sr and U-Th ages. Accessory phase crystallization appears to mainly document only minor changes in the magma chamber (changes in temperature) to which phases such as zircon or allanite are very sensitive. In contrast, the main phenocrysts, such as feldspar, record the major fractionation event.

6.6. Petrogenetic Model

A key to understanding the magmatic processes that generated the rhyolites at Long Valley lies in the long-term temporal evolution of the system associated with the rapid and episodic nature of rhyolite production (this study; Halliday et al., 1989; Christensen and DePaolo, 1993; Davies et al., 1994; Reid et al., 1997; Davies and Halliday, 1998). The rhyolites at Long Valley have been shown to be volatile rich (e.g., Wallace et al., 1999). In the subvolcanic environment at Long Valley, rising vapor pressure could cause rapid exsolution of a gas phase. Such a process of retrograde or secondary boiling is a common consequence of crystallization-dominated differentiation of magmas (Sisson and Bacon, 1999). The exsolution of gas can trigger gas-driven filter pressing, causing an effective separation of melts from crystals (Anderson et al., 1984). Sisson and Bacon (1999) have shown that gas-driven filter pressing occurs in vapor saturated silicic magmas at depth <10 km. A consequence of such a process would be to force highly evolved interstitial liquid from a crystal mush and in this way cause rapid magma differentiation. This process explains the generation of vapor-saturated, crystal-poor rhyolitic magmas because it accounts for the aphyric nature of many rhyolites, for the rapid production rates of rhyolites, and for the large inferred degrees of total fractional crystallization (low Sr contents; Halliday et al., 1991). The Long Valley magmatic system represents a batholith-scale magma volume (e.g., ~600 km^3 Bishop Tuff eruption at 750 ka). We conclude that effective separation of rhyolitic melts by gas-driven filter pressing at ~250 ka could have produced the volume of rhyolitic magmas that later formed the Deer Mountain and Mammoth Knolls Domes. When stored as melt lenses at the top of the magmatic reservoir, spatially separated from the main dynamic magma volume, these melts were thermally buffered by the underlying reservoir preventing complete solidification over a timescale of 150 ky. The reason that fractionated magmas can be stored without complete crystallization is the large size, longevity, and thermal gradient of the Long Valley silicic magma system. A schematic representation of these processes for the period 250 to 100 ky is given in Figure 10. A gas-driven filter pressing mechanism is probably faster and more efficient than previously proposed processes, such as permeability-controlled porous media flow through a solidification front (Trial and Spera, 1990). Currently, gas-driven filter pressing appears the best mechanism to explain high magma production rates recorded by rhyolites.

7. CONCLUSIONS

U-Th fractionation of postcaldera magmas at Long Valley is controlled by the accessory mineral phases zircon and allanite, which record extended preeruption residence times. Internal ^{230}Th-^{238}U isochrons corroborate Rb-Sr ages that indicate a major differentiation event at ~250 ka, 150 ky before eruption of the lavas, in a magmatic system of substantial longevity. The minor phases record no evidence of repeated heating-dissolution events. These data therefore require a relatively stable thermal regime with an integrated cooling rate of $<1 \times 10^{-3}$ °C /a. The inferred stable environment is in marked contrast to the implied dynamic open-system behavior of the postcaldera magmatic system over the past 700 ky. The data are best explained by isolation of small volumes of rhyolitic magma at the top of a large magma chamber, where they are physically isolated from the majority of the magma body. The main magma body is continuously fed by new magma, causing a temporal evolution in trace element and isotopic ratios. The open-system behavior supplies heat, preventing the entire system from complete solidification over the >700 ky of postcaldera magmatic activity.

Acknowledgments—Financial support was provided by the Vrije Universiteit and The Netherlands Organisation for Scientific Research. We gratefully acknowledge the assistance of C. van Belle, G. Koetsier, L. Ijlst, R. Smeets, and J. Wijbrans during sample preparation and analysis. The manuscript benefited from comments by S. Tommasini and constructive reviews by C. Bacon, B. Bourdon, and G. Mahood. This is NSG publication 20011005.

Associate editor: K. Mezger

REFERENCES

Allègre C. J. (1968) ^{230}Th dating of volcanic rocks. *Earth Planet. Sci. Lett.* **5,** 209–210.

Anderson A. T. J., Swihart G. H., Artioli G., and Geiger C. A. (1984) Segregation vesicles, gas filter-pressing, and igneous differentiation. *J. Geol.* **92,** 55–72.

Arth J. G. (1976) Behavior of trace elements during magmatic processes—A summary of theoretical models and their applications. *J. Res. U.S. Geol. Surv.* **4,** 41–47.

Bacon C. R. (1989) Crystallisation of accessory phases in magmas by local saturation adjacent to phenocrysts. *Geochim. Cosmochim. Acta* **53,** 1055–1066.

Bacon C. R., Persing H. M., Wooden J. L., and Ireland T. R. (2000) Late Pleistocene granodiorite beneath Crater Lake caldera, Oregon, dated by ion microprobe. *Geology* **28,** 467–470.

Bailey R. A. (1989) Geologic map of the Long Valley caldera, Mono-Inyo-Craters volcanic chain, and vicinity, eastern California. Map I-1933. U.S. Geological Survey.

Bailey R. A., Dalrymple G. B., and Lanphere M. A. (1976) Volcanism, structure, and geochronology of Long Valley caldera, Mono County, California. *J. Geophys. Res.* **81,** 725–744.

Barth S., Oberli F., and Meier M. (1989) U-Th-Pb systematics of morphologically characterized zircon and allanite: A high-resolution isotopic study of the Alpine Rensen pluton (northern Italy). *Earth Planet. Sci. Lett.* **95,** 235–254.

Barth S., Oberli F., and Meier M. (1994) Th-Pb versus U-Pb isotope systematics in allanite from co-genetic rhyolite and granodiorite:

implications for geochronology. *Earth Planet. Sci. Lett.* **124,** 149–159.

Blundy J. D. and Wood B. J. (1991) Crystal-chemical controls on the partitioning of Sr and Ba between plagioclase feldspar, silicate melts, and hydrothermal solutions. *Geochim. Cosmochim. Acta* **55,** 193–209.

Bohlen S. R., Eckert J. O., and Hankins W. B. (1995) Experimental determined solidi in the Ca-bearing granite system $NaAlSi_3O_8$-$CaAl_2Si_2O_8$-$KAlSi_3O_8$-SiO_2-H_2O-CO_2. *Am. Mineral.* **80,** 752–756.

Brown S. J. A. and Fletcher I. R. (1999) SHRIMP U-Pb dating of the preeruption growth history of zircons from the 340 ka Whakamaru Ignimbrite, New Zealand: Evidence for >250 ky magma residence times. *Geology* **27,** 1035–1038.

Cameron K. L. and Cameron M. (1986) Whole-rock/groundmass differentiation trends of rare earth elements in high-silica rhyolites. *Geochim. Cosmochim. Acta* **50,** 759–769.

Charlier B. and Zellmer G. (2000) Some remarks on U-Th mineral ages from igneous rocks with prolonged crystallisation histories. *Earth Planet. Sci. Lett.* **183,** 457–469.

Christensen J. N. and DePaolo D. J. (1993) Time scales of large volume silicic magma systems: Sr isotopic systematics of phenocrysts in glass from the Bishop Tuff, Long Valley, California. *Contrib. Mineral. Petrol.* **113,** 100–114.

Cousens B. L. (1996) Magmatic evolution of Quaternary mafic magmas at Long Valley Caldera and the Devils Postpile, California: Effects of crustal contamination on lithospheric mantle-derived magmas. *J. Geophys. Res.* **101,** 27673–27689.

Davies G. R., Halliday A. N., Mahood G. A., and Hall C. M. (1994) Isotopic constraints on the production rates, crystallisation histories and residence times of pre-caldera silicic magmas, Long Valley, California. *Earth Planet. Sci. Lett.* **125,** 17–37.

Davies G. R. and Halliday A. N. (1998) Development of the Long Valley rhyolitic magma system: Strontium and neodymium isotope evidence from glasses and individual phenocrysts. *Geochim. Cosmochim. Acta* **62,** 3561–3574.

Duffield W. A., Ruiz J., and Webster J. D. (1995) Roof-rock contamination of magma along the top of the reservoir for the Bishop Tuff. *J. Volcanol. Geotherm. Res.* **69,** 187–195.

Freer R. (1981) Diffusion in silicate minerals and glasses: A data digest and guide to the literature. *Contrib. Mineral. Petrol.* **76,** 440–454.

Giletti B. J. (1990) Mg, Ca, Sr, and Ba diffusion in plagioclase and Sr diffusion in micas. *Eos* **72,** 292.

Goldstein S. J., Murrell M. T., and Janecky D. R. (1989) Th and U isotopic systematics of basalts from the Juan de Fuca and Gorda Ridges by mass spectrometry. *Earth Planet. Sci. Lett.* **96,** 134–146.

Halliday A. N., Mahood G. A., Holden P., Metz J. M., Dempster T. J., and Davidson J. P. (1989) Evidence for long residence times of rhyolite magma in the Long Valley magma system: The isotopic record in the precaldera rhyolite lavas of Glass Mountain. *Earth Planet. Sci. Lett.* **94,** 274–290.

Halliday A. N., Davidson J. P., Hildreth W., and Holden P. (1991) Modelling the petrogenesis of high Rb/Sr silicic magmas. *Chem. Geol.* **92,** 107–114.

Harrison T. M. and Watson E. B. (1983) Kinetics of zircon dissolution and zirconium diffusion in granite melts of variable water content. *Contrib. Mineral. Petrol.* **84,** 66–72.

Heumann A. (1999) Longevity of silicic magma chambers. Ph.D. thesis. Vrije Universiteit, Amsterdam.

Heumann A. and Davies G. R. (1997) Isotopic and chemical evolution of the postcaldera rhyolitic system at Long Valley, California. *J. Petrol.* **38,** 1661–1678.

Hildreth W. (1979) *The Bishop Tuff: Evidence for the Origin of Compositional Zonation in Silicic Magma Chambers.* Special Paper 180. Geological Society of America.

Holden N. E. (1989) Total and spontaneous fission half-lives for uranium, plutonium, americium and cerium nuclides. *Pure Appl. Chem.* **61,** 1483–1504.

Knesel K. M. and Davidson J. P. (1997) The origin and evolution of large-volume silicic magma systems: Long Valley caldera. *Internat. Geol. Rev.* **39,** 1033–1052.

Knesel K. M., Davidson J. P., and Duffield W. A. (1999) Evolution of silicic magma through assimilation and subsequent recharge: Evidence from Sr isotopes in sanidine phenocrysts, Taylor Creek Rhyolites, NM. *J. Petrol.* **40,** 773–786.

Lowenstern J. B., Persing H. M., Wooden J. L., Lanphere M., Donnelly N. J., and Grove T. L. (2000) U-Th dating of single zircons from young granitoid xenoliths: New tools for understanding volcanic processes. *Earth Planet. Sci. Lett.* **183,** 291–302.

Mahood G. A. and Hildreth W. (1983) Large partition coefficients for trace elements in high-silica rhyolites. *Geochim. Cosmochim. Acta* **47,** 11–30.

Mankinen E. A., Gromme C. S., Dalrymple G. B., Lanphere M. A., and Bailey R. A. (1986) Paleomagnetism and K-Ar ages of volcanic rocks from Long Valley caldera, California. *J. Geophys. Res.* **91,** 633–652.

McIntyre G. A., Brooks C., Compston W., and Turek A. (1966) The statistical assessment of Rb-Sr isochrons. *J. Geophys. Res.* **71,** 5459–5468.

Metz J. and Mahood G. A. (1985) Precursors to the Bishop Tuff eruption: Glass Mountain, Long Valley, California. *J. Geophys. Res.* **90,** 11121–11126.

Michael P. (1988) Partition coefficients for rare earth elements in mafic minerals of high silica rhyolites: The importance of accessory mineral inclusions. *Geochim. Cosmochim. Acta* **52,** 275–282.

Montel J.-M. (1993) A model for monazite/melt equilibrium and application to the generation of granitic magmas. *Chem. Geol.* **110,** 127–146.

Nash W. P. and Crecraft H. R. (1985) Partition coefficients for trace elements in silicic magmas. *Geochim. Cosmochim. Acta* **49,** 2309–2322.

Pringle M. S., McWilliams M., Houghton B. F., Lanphere M. A., and Wilson C. J. N. (1992) $^{40}Ar/^{39}Ar$ dating of Quarternary feldspar: Examples from the Taupo Volcanic Zone, New Zealand. *Geology* **20,** 531–534.

Reid M. R., Coath C. D., Harrison T. M., and McKeegan K. D. (1997) Prolonged residence times for the youngest rhyolites associated with Long Valley caldera: ^{230}Th-^{238}U ion microprobe dating of young zircons. *Earth Planet. Sci. Lett.* **150,** 27–39.

Reid M. R. and Coath C. D. (2000) In situ U-Pb ages of zircons from the Bishop Tuff: No evidence for long crystal residence times. *Geology* **28,** 443–446.

Sampson D. E. and Cameron K. L. (1987) The geochemistry of the Inyo volcanic chain: Multiple magma systems in the Long Valley region, eastern California. *J. Geophys. Res.* **92,** 10403–10421.

Shaw H. R. (1985) Links between magma–tectonic rate balances, plutonism, and volcanism. *J. Geophys. Res.* **90,** 11275–11288.

Simkin T. (1993) Terrestrial volcanism in space and time. *Ann. Rev. Earth. Planet. Sci.* **21,** 427–452.

Sisson T. W. and Bacon C. R. (1999) Gas-driven filter pressing in magmas. *Geology* **27,** 613–616.

Spera F. J. and Crisp J. A. (1981) Eruption volume, periodicity and caldera area: Relationships and inferences on development of compositional zonation in silicic magma chambers. *J. Volcanol. Geotherm. Res.* **11,** 169–187.

Sun S. S. and Hanson G. N. (1975) Origin of Ross Island basanitoids and limitations on the heterogeneity of mantle sources for alkali basalts and nephelinites. *Contrib. Mineral. Petrol.* **52,** 77–106.

Taddeucci A., Broecker W. S., and Thurber D. L. (1967) ^{230}Th dating of volcanic rocks. *Earth Planet. Sci. Lett.* **3,** 338–342.

Titterington D. M. and Halliday A. N. (1979) On the fitting of parallel isochrons and the method of maximum likelihood. *Chem. Geol.* **26,** 183–195.

Trial A. F. and Spera F. J. (1990) Mechanisms for the generation of compositional heterogeneities in magma chambers. *Geol. Soc. Am. Bull.* **102,** 353–367.

Vogel T. A., Eichelberger J. C., Younker L. W., Schuraytz B. C., Horkowitz J. P., Stockman H. W., and Westrich H. R. (1989) Petrology and emplacement dynamics of intrusive and extrusive rhyolites of Obsidian Dome, Inyo Craters volcanic chain, eastern California. *J. Geophys. Res.* **94,** 17937–17956.

Vogel T. A., Woodburne T. B., Eichelberger J. C., and Layer P. W. (1994) Chemical evolution and periodic eruption of mafic lava flows in the west moat of Long Valley Caldera, California. *J. Geophys. Res.* **99,** 19829–19842.

Wallace P. J., Anderson A. T., and Davis A. M. (1999) Gradients in H_2O, CO_2, and exsolved gas in a large-volume silicic magma system: Interpreting the record preserved in melt inclusions from the Bishop Tuff. *J. Geophys. Res.* **104,** 20097–20122.

Watson E. B. and Harrison T. M. (1983) Zircon saturation revisited: Temperature and composition effects in a variety of crustal magma types. *Earth Planet. Sci. Lett.* **64,** 295–304.

Wijbrans J. R., Pringle M. S., Koppers A. A. P., and Scheveers R. (1995) Argon geochronology of small samples using the Vulkaan argon laserprobe. *Proc. Kon. Ne. Akad. Wetensch.* **98,** 185–218.

York D. (1969) Least squares fitting of a straight line with correlated errors. *Earth Planet. Sci. Lett.* **5,** 320–324.